# Geometric Optimization of Controlled Collapse Interconnections\*

Abstract: This paper deals with the mechanical reliability of controlled collapse solder joints in modules subjected to the thermal fatigue conditions of machine usage. Particular emphasis is placed on design variability and how the shape and dimensions of the joint and chip affect reliability. A systematic technique is presented to optimize pad dimensions. A new experimental method to characterize chip-to-substrate interconnections—the torque test—is described and analyzed. Its applicability to design evaluation is discussed and representative data are analyzed. The relationship between torque test measurements and fatigue is discussed.

#### Introduction

Theory is presented relating to geometric optimization of controlled collapse chip joints, with the aim of reducing local shear strains arising in a machine environment and hence increasing the cyclic fatigue life of the joints. The need is emphasized for a compliant (ductile) joint in the bulk solder, and for high strength in the vicinity of the interfaces with chip and substrate. Before beginning the extended discussion, we present a brief summary of the method.

The joint may be optimized in the following manner:

- (1) Determine experimentally the ratio of the land area,  $\pi r_0^2$  (joint-substrate interface), to chip metallization area,  $\pi r_1^2$  (joint-chip interface), for which fractures are evenly divided between the two interfaces. Thermal cycling or torque testing may be utilized to determine this ratio K. This ratio is then the optimum for design purposes. If it is assumed that the radius  $r_1$  of the chip metallization (ball-limiting metallization, or BLM) has been fixed and K determined, the optimum land is then a square with side  $2r_0^* = \sqrt{Kr_1}$ .
- (2) Measure or estimate the strain-hardening exponent  $\beta$  of the pad. If 5/95 Sn/Pb solder is used, a working value for  $\beta$  is 0.58 for chips 40 to 120 mils on a side.
- (3) The optimum value of the solder volume of the joint is then given by Eq. (11) or Fig. 12 (see the following discussion)

For example, assume  $r_1$  is fixed at 2 mils, i.e., that the chip metallization has a diameter of 4 mils, and that K = 1.59. Then  $r_0^* = 2.525$ , or the optimum land size is

 $5.05 \times 5.05$ . Now, if a nominal  $5 \times 5$  land is chosen, the optimum solder volume may be found from Fig. 12, with  $r_1 = 2$ ,  $r_0 = 2.5$ ,  $\beta = 0.58$ :  $V^* = 81 \text{ mil}^3$ . The optimum joint will then have the appearance of Fig. 1 with a solder height, h, of 3.5 mils.

Commercial screening and device fabrication processes are readily capable of achieving optimum joint dimensions.

#### • The controlled collapse joint

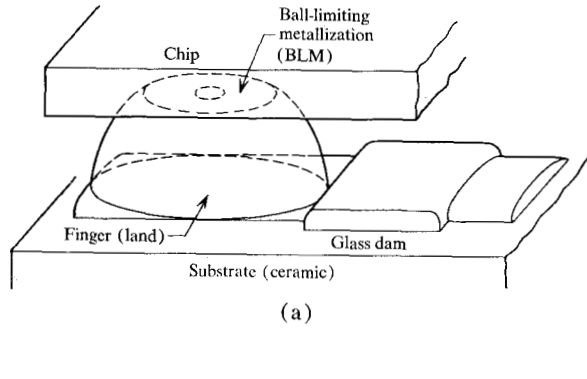
The controlled chip collapse joining technique is described in a companion paper. By this process, solder on the chip and a tinned electrode on the substrate are placed in juxtaposition and the system is reflowed, resulting in a single solder joint, or pad. Surface tension insures good alignment and provides positive support for the chip. Spreading is limited on the chip by a specially designed contact, the "ball-limiting metallization" (BLM) and, typcially, on the substrate by a glass dam. A typical completed joint is shown in the top sketch of Fig. 1.

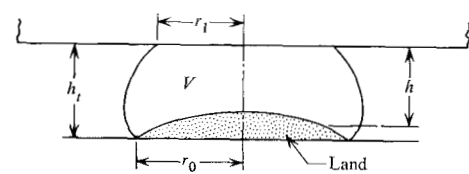
In machine operation, as the temperature of the module increases, unequal expansion between the chip and ceramic substrate results in a shear displacement between the top and bottom of each pad. Moreover, the displacement is removed and reapplied each time the machine is turned off and on.† If the imposed stress or strain is beyond some

The author is located at the IBM Components Division Laboratory, E. Fishkill, New York.

<sup>\*</sup> A briefer version of this paper was presented at the 1969 Electronic Components Conference, IEEE (G-PMP) and Electronic Industries Association, Washington, D.C., April 30-May 2, 1969.

<sup>†</sup> Variations in temperature arising during a machine on-cycle are very small compared to turn-on and turn-off perturbations and are therefore not considered significant in fatigue life.





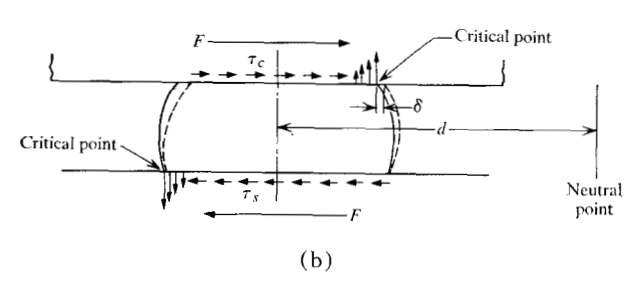


Figure 1 Schematic of joint and definitions: (a) threedimensional sketch; (b) sections before and after thermal displacement.

critical level, repeated cycling will eventually cause mechanical rupture of the joint and consequent electrical discontinuity. It is thus important to be able to design the pad in such a way as to minimize the likelihood of failure within the lifetime of the equipment containing the component, and to have some technique by which this likelihood can be evaluated experimentally.

This paper discusses how the joint may be designed to best resist fatigue degradation; specific conditions and systematic procedures are given. It is shown, furthermore, how design and manufacturing variations resulting in deviations from joint optimization affect cyclic fatigue life. A mechanical test is introduced which can rapidly predict qualitative fatigue life, and its application in one step of joint optimization is described.

This paper will not discuss evaluation of actual fatigue life in a machine environment; nor is it concerned with acceleration factors between real-time and various simulated thermal fatigue cycles. It is recognized that such factors as temperature rise times, dwell times, and maximum and minimum temperatures encountered in the operating environment greatly influence fatigue life. These

effects, however, are discussed elsewhere.<sup>2</sup> It is only the relative fatigue life of different designs which is of concern here.

#### • Definitions, assumptions, and nomenclature

A schematic drawing of a typical controlled collapse joint is shown in Fig. 1, with pertinent parameters labeled. Since the substrate land finger is nominally rectangular, the completed joint has a rectangular shape at the very bottom, but becomes circular in cross section almost immediately above the base. For this reason the pad can conveniently be analyzed as a solid of rotation, having a circular section at every height. The ball-limiting metallization (the solder wetting area on the chip) is circular with radius  $r_1$ , and the effective finger radius\* is defined as  $r_0$ . The layer of electrode land (Ag-Pd) under the joint is much stiffer than the solder, and for stress-strain purposes it is important to distinguish between the solder height h and the total chip-to-substrate height  $h_t$ ; and between the solder volume V and the total solder-plusland volume  $V_t$ . In the analysis, it will be assumed that the entire thermal displacement is borne by the solder.

Another drawing in Fig. 1 defines the shear force F and shear stresses,  $\tau_c$  and  $\tau_s$ . Normal stresses are also shown to be exerted by the chip and substrate on the corners of the pad, and it may be easily seen that these stresses must exist if the joint is to stay in rotational equilibrium (moment balance). Testing has shown that fractures in thermal fatigue or in single-cycle mechanical tests usually begin at one of these high-stress points, where normal tension and shear components are superimposed. The magnitude of the normal stresses in the plastic and fatigue modes is not known at present, but it can be assumed they are approximately proportional to the average shear stress along the interface.<sup>†</sup> Thus the shear stress can be used as a comparative stress value, if it is understood that physically it is not the sole direct fracture stress.

The solder volume V is by no means composed only of lead and tin, but contains impurities from the ball-limiting metallization and from the land. The resulting structure of alloys and intermetallics is quite complex and inhomogeneous, but for this analysis it is idealized as being a homogeneous pad having gross, macroscopic properties.

A complete list of nomenclature follows:

 $r_0$  = effective finger radius;

 $r_1 = BLM \text{ radius};$ 

 $r_t$  = radius of critical interface

h =solder height of joint;

 $h_t$  = total chip-to-substrate height;

V =solder volume of ioint;

<sup>\*</sup> For square fingers (length = width),  $r_0 = 0.5 \times$  width; for rectangular fingers (length  $\neq$  width),  $r_0 = 0.5 \sqrt{\text{length} \times \text{width}}$ .

<sup>†</sup> The effect of the contact angle on normal stresses is discussed briefly in Appendix B.

 $V_t$  = total solder-plus-land volume;

 $\tau_c$  = average shear stress at chip-pad interface;

 $\tau_{\bullet}$  = average shear stress at land-substrate interface;

F = shear force;

 $\gamma_c$  = local shear strain in solder near chip;

 $\gamma_{\bullet}$  = local shear strain in solder near land;

 $\gamma$  = average shear strain of joint;

= shear deformation of joint;

 $\alpha$  = differential thermal expansivity, Si vs. ceramic;

 $\Delta T$  = change in temperature;

 d = distance of joint from neutral or stationary point of chip;

 $\bar{d}$  = average value of d for all joints on a chip;

n =the number of joints on a chip;

 $A, \beta =$ constants in stress-strain relationship  $\tau = A\gamma^{\beta}$ ;

 $\beta_d$  = design value of  $\beta$  for minimum deviation from maximum cyclic fatigue life;

 $\beta'$  = minimum value of  $\beta$  for joint;

\* = a symbol to indicate the optimized value of a parameter;

 $R_h = h/h^*$ ;

 $R_V = V/V^*;$ 

 $\theta_1$  = contact angle at chip;

 $\theta_0$  = contact angle at substrate;

 $T_m$  = peak torque in torque test, expressed as shear load per joint;

 $\phi_m$  = angle to which chip must be twisted to reach the peak torque;

 $N_f$  = number of cycles to joint fracture in a fatigue or machine cycle;

m =exponent in the Coffin-Manson equation;

 $K_T$  = constant in applied Coffin-Manson equation, a function only of the parameters of the testing cycle;

 $\tau_{ue}$  = ultimate shear strength of the chip-pad interface in lb/in.<sup>2</sup>:

 $\tau_{us}$  = ultimate shear strength of the land-substrate interface in lb/in.<sup>2</sup>;

 $K = \tau_{uc}/\tau_{us}$ ; and

 $\tau_u$  = ultimate shear strength of the critical interface (equal to  $\tau_{ue}$  or  $\tau_{ue}$  depending on predominant fracture mode).

It is assumed that the solder joint can be treated analytically as a homogeneous unit, except for the land. Further, it is assumed that the Coffin-Manson fatigue equation, with local shear strain as the parameter, is valid; and that the shear stress-shear strain characteristic of the pad is as shown in Fig. 2. Finally, it is assumed that due to the low yield point of solder, the plastic strain component in any fatigue cycle of interest is far greater than the elastic component.

Throughout this paper the term fracture will be used to denote either the start of fracture or complete fracture

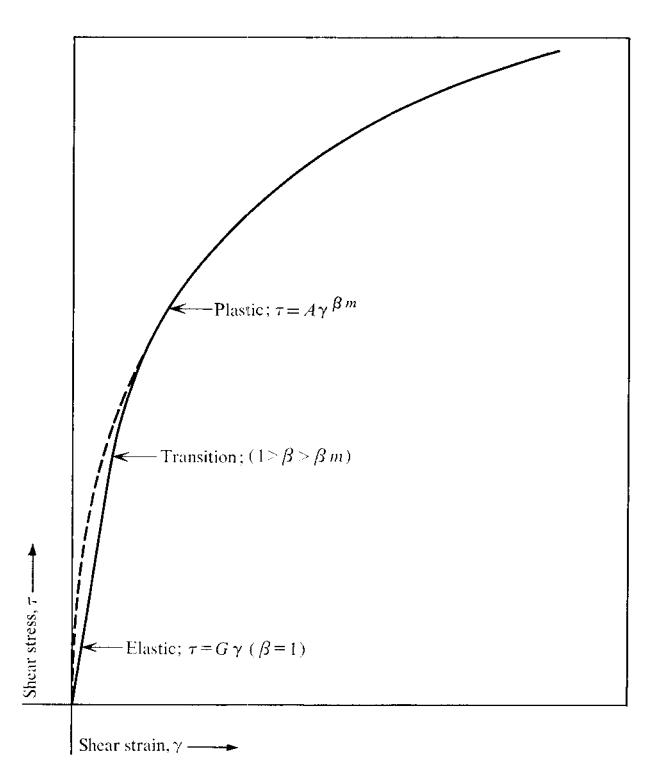


Figure 2 Idealized stress-strain curve in shear for solders.

(electrical "open") depending on the context. It will be assumed that a fracture which starts at a particular interface (say that between land and ceramic) of a joint will completely traverse the joint before a crack will form at the opposite interface, and further that if two joints are subjected to a particular fatigue environment, the one that begins to fracture first will complete fracture first.

#### Theoretical and experimental techniques

#### • The basic equation

The Coffin-Manson equation, with local shear strain as the determinant parameter, has been manipulated in Appendix A to obtain an equation directly applicable to joint fatigue. Equation (A9) is

$$N_f = K_T \left( \tau_u \pi r_f^2 \frac{h^{1+\beta}}{A V} \right)^{m/\beta} \left( \frac{1}{\delta} \right)^m , \qquad (1)$$

where  $\tau_u$  and  $r_f$  refer to the ultimate shear strength and radius at the critical cross section or interface of the pad. Failures in thermal cycling and torque test (to be discussed later) occur predominantly in one of two modes: (1) starting at the chip-joint interface, cracks propagating through the solder adjacent to the ball-limiting metallization or between the BLM and glass; and (2) cracking along the land-ceramic interface. Other modes occur rarely and will be excluded from this analysis. The two predominant modes

253

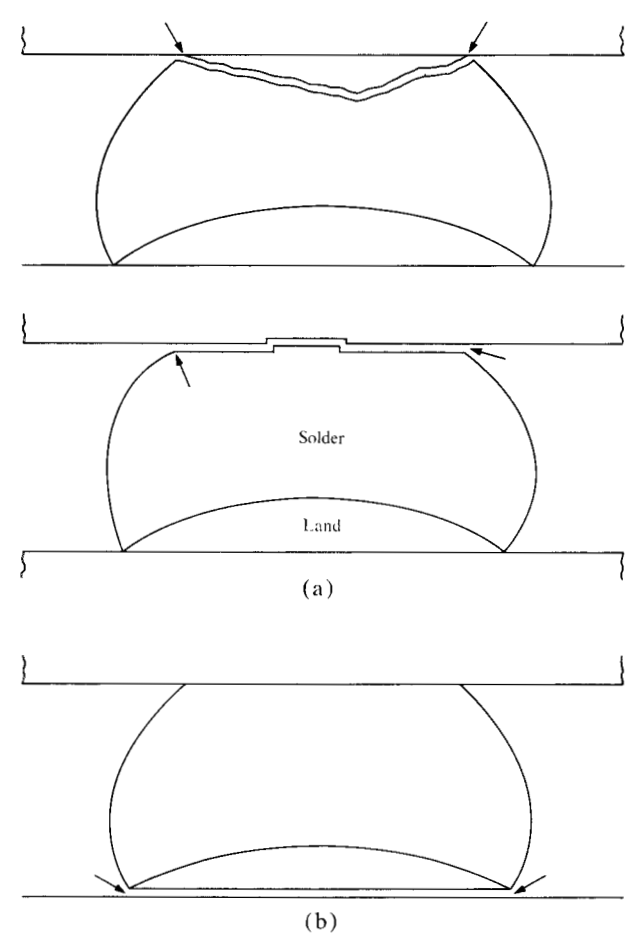
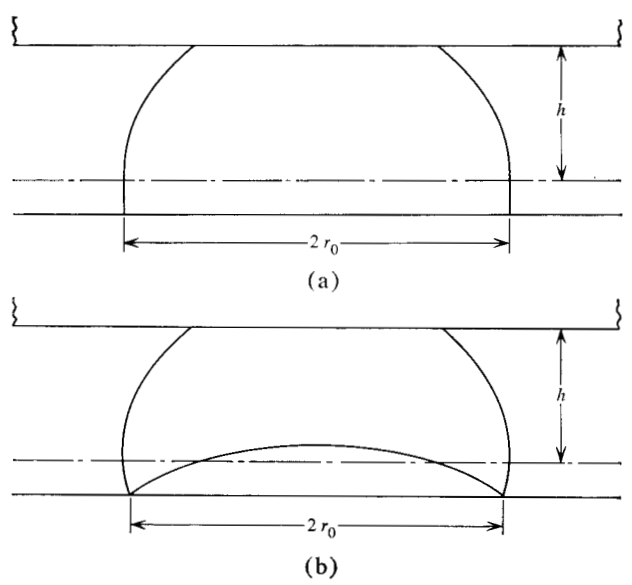


Figure 3 Principal modes of fracture of controlled collapse joint (arrows indicate points at which fractures initiate).

(a) Chip fractures; (b) substrate fracture.

Figure 4 (a) Idealized shape of controlled collapse joint; (b) actual shape.



of interest are illustrated in Fig. 3 and will be referred to as "chip" and "substrate" fractures respectively. In the case of thermal cycling, in which stresses alternate every half cycle, fractures proceed inward from both ends of the critical interface.

The failure mode that predominates depends to a great extent on the ratio of chip BLM area and substrate land (finger) area, i.e., on the ratio  $r_1/r_0$ . For any set of substrate and chip processing conditions, there is some value of this ratio for which the failure modes are equalized. This ratio is defined as  $\sqrt{K}$ , and it is a simple matter to show that  $K = \tau_{uc}/\tau_{us}$ , the ratio of ultimate shear strengths of the chip-joint and joint-substrate interfaces, respectively. If  $r_0 < \sqrt{K}r_1$ , substrate fractures predominate, and in Eq. (1)  $r_f = r_0$  and  $\tau_u = \tau_{us} = \tau_{uc}/K$ . If on the other hand  $r_0 > \sqrt{K}r_1$ , chip fractures predominate,  $r_f = r_1$ , and  $\tau_u = \tau_{uc}$ . Equation (1) may then be rewritten

$$N_{f} = K_{T} \left(\frac{1}{\delta}\right)^{m} \cdot \left[\frac{h^{1+\beta}}{A V} \tau_{uc} \pi \begin{bmatrix} r_{1}^{2} & \text{for} \quad r_{0} > \sqrt{K} r_{1} \\ r_{0}^{2}/K & \text{for} \quad r_{0} < \sqrt{K} r_{1} \end{bmatrix}\right]^{m/\beta}. \quad (2)$$

It is apparent that to optimize the fatigue life of controlled collapse joints, the large term in brackets must be maximized. There are two parts to this term, and it is of great interest to study these separately.

#### The interplay of strength and stiffness

The term  $\tau_u \pi r_f^2$  in Eq. (1) is the ultimate shear force of the joint, that shear load at which the first noticeable crack starts. It is of course beneficial for this term to be as large as possible. The term  $h^{1+\beta}/AV$  may be shown to be related to the reciprocal of the joint stiffness\*; and it is therefore desirable to minimize the joint stiffness or, in other words, to maximize joint flexibility or compliance. The interplay of these two factors—minimizing stiffness while maximizing ultimate strength—is the basic concept in the mechanical aspect of joint design. Note that for a bulk material these conditions are usually antitheticalgreater strength is usually accompained by brittleness, and greater ductility by lower ultimate strength. However, the particular system of the controlled collapse joint has high intermetallic concentrations near the interfaces for strength, and relatively pure solder in the bulk section of the pad for compliance, allowing the above conditions to be met and effective optimization to be attained.

## • Elaboration of parameters in basic equation It is to be noted that the parameters h and V in Eq. (2)

<sup>\*</sup> In the elastic case  $\beta=1$  and A=G, the shear modulus. This term then becomes  $h^2/VG$  which is the exact expression for the compliance of a right circular cylinder.

refer to the height and volume of the solder portion of the controlled collapse joint. This assumes that the electrode land is much stiffer than the solder, such that the latter must absorb the entire thermal displacement on the joint. From the sketch in Fig. 1 it is apparent that h is not easily defined since the land is not of uniform height. Thus for the purposes of optimization the joint is idealized as an electrode layer of uniform thickness, topped by a solder pad as shown in Fig. 4. This approximation is very accurate for optimization; modifications must be made, however, when curves of  $N_f$  versus some geometrical parameter are plotted and the land height is more than one third the total chip-to-substrate height.\*

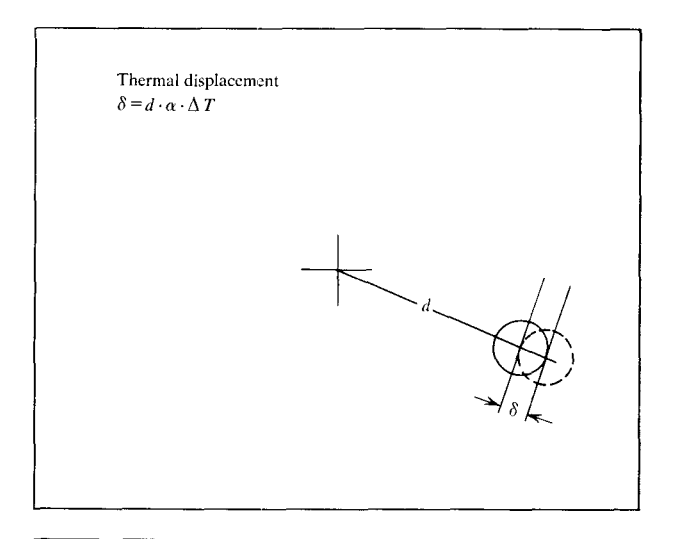
The displacement  $\delta$  in Eq. (2) is equal to  $d\alpha\Delta T$ , where  $\alpha$  is the thermal mismatch (difference in thermal expansivities) between the silicon chip and ceramic substrate,  $\Delta T$  the temperature change of the system, and d the distance of the joint in question from the neutral or stationary point—that point on the chip which does not move relative to the substrate. When all joints are identical (which is the case considered in this paper) and if they are more or less uniformly spaced around the periphery of the chip, the neutral point is approximately at the geometric center of the chip. Thus d is a measure of chip size. If the chip and substrate are at different temperatures—a situation not unlikely in a machine environment—this must be taken into account when computing  $\delta$ .

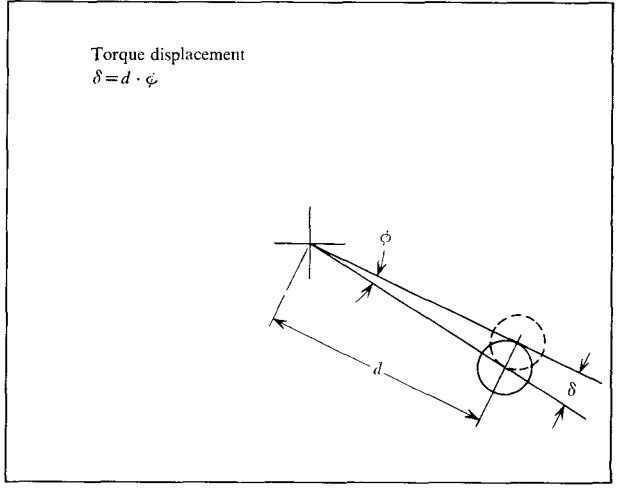
#### • The torque test

At this point we digress from the theoretical analysis, to discuss the testing of controlled chip collapse interconnections. It is obviously very desirable to have a rapid test, destructive if necessary, which can evaluate those properties of the joints that are critical in machine cycling, and thus to be able to assess, if only qualitatively, the resistance to cyclic fatigue of the configuration in question. A torque test fulfills these criteria.

It was shown in the first section of this study that a pad exposed to a thermal environment "sees" a shear displacement proportional to its distance from the neutral point. Thus a mechanical test which simulates a thermal cycle is required (a) to place each pad in shear; (b) to be able to measure or control the displacement on each pad; and (c) to strain each pad to an extent proportional to its distance from the neutral point.

These criteria are fulfilled if the chip is twisted: a shear displacement is applied to each pad; a sufficiently long torque arm can magnify the displacement such that it can be accurately measured; and if the center of twist is at the neutral point, the displacement is proportional to its distance from the neutral point. The correspondence between thermal cycle and torque displacement is shown in





For correspondence,  $\phi = \alpha \Delta T$ 

Figure 5 Torque-temperature correspondence.

Fig. 5. In practice the neutral point for a chip with symmetrically placed pads is very close to the geometric chip center. Fig. 5 shows that if a twist  $\phi$  equal numerically to  $\alpha \Delta T$  is applied, each pad has nominally the same shear displacement imposed upon it as if it were exposed to a system temperature change of  $\Delta T$ . In one case the displacement is along the line joining the pad to the chip center; in the other it is perpendicular to this line. However the radial symmetry of the pad justifies the correspondence.

In the torque tester built and in operation at the author's location, a stem is cemented to the top of the chip and clamped to the frame. The module rests in a vise which is magnetically held to a frictionless torque arm. The arm, twelve inches long, is driven at known speed by a force transducer whose output is recorded on the ordinate of an x-y recorder. The x scale is a time sweep, which is proportional to arm displacement. Thus an x-y

<sup>\*</sup> This case is still being studied and will not be discussed in this paper.

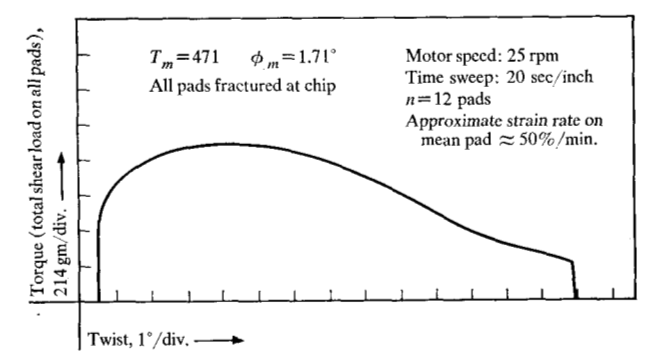


Figure 6 A typical torque test curve.

plot gives us a torque versus twist curve. A typical output curve is shown in Fig. 6, with conversion factors indicated.

Since the test measures only collective properties of the n joints on a chip, it is convenient to define a hypothetical "mean pad" located a distance  $\bar{d}$  from the center of the chip, where  $\bar{d}$  is the average distance of the n pads from the center.\*

The torque test curve has a typically repeatable shape, resembling in its early stage the stress-strain curve in shear (Fig. 2). Fracture on the mean pad begins near the peak of the curve, and physically starts at a corner of the padchip or land-substrate interface at the points indicated by arrows in Fig. 3. Complete fracture on the most distant pad (the most critical) occurs well past the peak, for example about 3° past it in the curve shown. Thus the torque test cannot detect a complete pad fracture, but only the point at which the mean pad begins to fracture.

Two figures of merit are taken in the test: the peak torque  $T_m$  and the angular twist  $\phi_m$  at which  $T_m$  occurs.  $T_m$  is generally expressed as a net ultimate shear load on all pads, to enable comparison with the pull test value (the force required to pull the chip from the substrate) to which it is analogous. Typically, controlled collapse joints can sustain 20-35 grams per pad maximum shear load.

Equation (1) may be modified for the case when the cycle in question is a twist to destruction. It is assumed that the neutral point in thermal cycling is the geometric center of the chip. The ultimate shear load per pad,  $T_m$ , is exactly equal to  $\tau_n \pi r_t^2$  and the displacement  $\delta$  of the mean pad is

\* Theoretically this distance should be

$$\bar{d} = \left(\sum_{i=1}^{n} d_i^{1+\beta}\right) / \left(\sum_{i=1}^{n} d_i^{\beta}\right),$$

but to an extremely close approximation,

$$\bar{d} pprox rac{1}{n} \sum_{i=1}^{n} d_i$$
.

 $\phi \bar{d}$ . When  $\phi = \phi_m$ , fracture begins in one-half cycle. Thus, rearranging Eq. (1), we have

$$\phi_m = (2 K_T)^{1/\beta_m} \frac{1}{\bar{d}} \left( \frac{T_m}{A} \frac{h^{1+\beta}}{V} \right)^{1/\beta}.$$

Now, at fracture, it is apparent that the critical local stress has reached the ultimate. Thus from equation (A6) in Appendix A,  $K_T = 1/2$ , and

$$\phi_m = \frac{1}{d} \left( \frac{T_m}{A} \frac{h^{1+\beta}}{V} \right)^{1/\beta}. \tag{3}$$

The term in parentheses is identical to the corresponding term in Eq. (1). Therefore, the same parameters which influence  $N_f$  also influence  $\phi_m$  in a torque test, and in the same way.

Allowing for the approximations in derivation, and for the fact that in thermal cycling we measure complete fracture while  $\phi_m$  marks only the start of fracture, we can nevertheless assume that the number of cycles to thermal fatigue failure in a fixed cycle is a monotonically increasing function of  $\phi_m$  as measured in a torque test. A sample that exhibits greater twist-to-peak torque values than another can therefore be expected to survive longer in thermal cycling. Moreover, this comparison can theoretically be made among different chip sizes, solders, and in general among different module designs, as well as among variants within the same design.

The universal relationship between  $N_f$  and  $\phi_m$  is at present unverified experimentally, although all data collected to date have indicated that units with low  $\phi_m$  tend to degrade more quickly in thermal fatigue. The summarized data on one particular design are illustrated in Fig. 7, where the median failure point of units cycled from 0 to 150°C is plotted against  $\phi_m$  (average of 5-10 chips) for units from the same group measured in a torque test. Each group tested represents a geometric, metallurgical, or process variation from the nominal design. The predictive capabilities of the torque test are apparent from this curve.

The torque test, as well as being able to qualitatively monitor the fatigue resistance of a product sample, can often be used to pinpoint suspect areas when product degradation is indicated. As an example, average data for joints with different electrode pastes, but otherwise identical, are shown in Table 1. Since the ultimate strengths of the three groups are about the same, it is apparent that the difference in  $\phi_m$  can be traced to stiffness factors, group A having lower stiffness than B, which is in turn more compliant than C. It was subsequently discovered that pastes B and C spread on the substrate more than A causing the chip to drop lower and resulting in a lower  $h^{1+\beta}/V$  ratio; also these pastes tended to spall intermetallics into the joint during joining more than did paste A. Both of these factors would tend to produce the differences noted.

Table 1 Torque test data for designs with different electrode pastes.

Paste	$\phi_m$ , degrees (average)	T <sub>m</sub> , grams shear load per pad (average)		
Α	2.05	33.3		
В	1.71	35.1		
C	1.48	33.7		

If a decrease in  $\phi_m$  is accompanied by like changes in  $T_m$ , it is not readily apparent whether the drop in  $\phi_m$  is due entirely to the lower ultimate strength, or whether stiffness factors are also involved. Much can be learned, however, from a rearrangement of Eq. (3):

$$\ln\left(\frac{\phi_m \bar{d}}{h}\right) = \frac{1}{\beta} \left[ \ln\left(\frac{T_m h}{V}\right) - \ln A \right]. \tag{4}$$

Thus if  $\ln (T_m h/V)$  is plotted against  $\ln (\phi_m \bar{d}/h)$  for different samples tested, a straight line with slope  $\beta$  indicates changes in ultimate strength and geometry (different h or V). Points off the line indicate changes in the bulk solder properties. An example is shown in Fig. 8 in which, as before, each point represents an average of 5-10 chips. Most points fall on the line of  $\beta=0.35$ , which agrees well with values measured from actual expanded torque-twist curves. Areas indicating either stiffer or more compliant gross joint solder are indicated. A cursory analysis of the fracture mode of the samples represented by points falling on the line usually can pinpoint the cause of the change in ultimate strength.

If joint dimensions are not known from production data or from microsections,  $\ln \phi_m$  may be plotted against  $\ln T_m$  and a similar curve will result, although points off the curve may in this case indicate dimensional changes as well as changes in A and  $\beta$ .

For torque testing to be useful in predicting qualitative fatigue behavior, three conditions must hold. First, the percentage of chip and substrate pad fractures in the torque test should approximately equal the percentage of chip and substrate fractures in machine cycling. In addition, in any fatigue test with a fixed cycle in which any two variations of a controlled collapse joint are compared, a joint which on the average begins to fracture earliest must complete fracture earliest. In other words, torque testing measures only the start of fracture, and if modules "A" have a lower  $\phi_m$  than modules "B", this indicates that in a fatigue test, pads of module "A" will begin to fracture at a lower number of cycles than "B." If the test is to be meaningfully correlated with fatigue, "A" must also complete fracture prior to "B." Intuitively and theoreti-

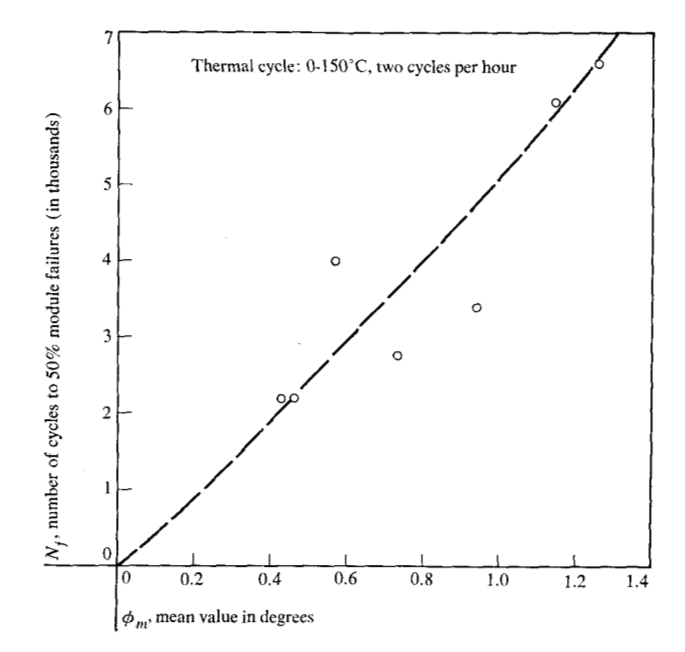
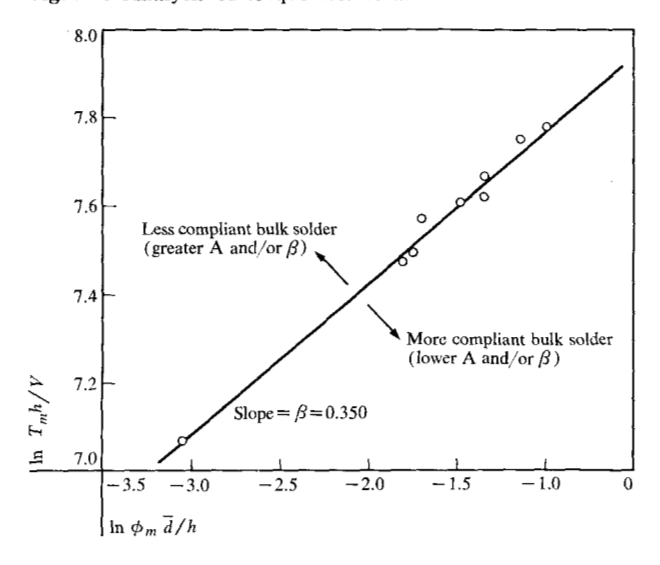


Figure 7 Curve showing the correlation between  $N_t$  and  $\phi_m$ .

Figure 8 Analysis of torque test data.



cally this should be the case, and correlative torquefatigue data collected to date (as in Fig. 7) have so affirmed. Finally, no extensive metallurgical reactions should take place in the thermal or machine cycle of interest.

To summarize, the torque test is a technique which can rapidly monitor design consistency or evaluate design or process changes with regard to predicted fatigue life, and can conveniently isolate the ultimate strength and stiffness factors when changes are encountered. Its use in the determination of optimum interface dimensions will be described in the following section.

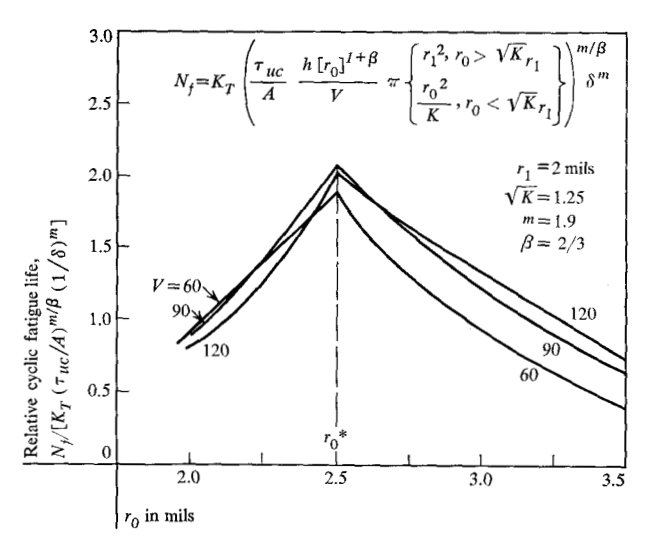


Figure 9 Relative joint fatigue life (theoretical) vs. finger size.

### Optimizing joint dimensions for maximum cyclic fatigue life

#### Natural shape of controlled collapse chip joint

The shape of the pad is fully defined by the four dimensional parameters  $r_0$ ,  $r_1$ ,  $h_t$  and  $V_t$ . However, it has been shown theoretically and verified by numerous microsections that if all pads joining a chip to a substrate are identical and if the weight of the chip is not excessive, then each pad has a shape approximated by a spherical segment. Thus the dimensional parameters are not mutually independent but related by the equation

$$V_t = \frac{\pi h_t}{6} \left[ h_t^2 + 3(r_0^2 + r_1^2) \right]. \tag{5}$$

The approximation illustrated in Fig. 4 can now be applied to this equation, resulting in the same relationship between solder height and volume:

$$V = \frac{\pi h}{6} \left[ h^2 + 3(r_0^2 + r_1^2) \right]. \tag{6}$$

As noted earlier, this idealization is not too accurate when paste heights are large compared to  $h_t$ , but it is excellent for purposes of dimensional optimization. In the analysis to follow, the spherical segment geometry is used exclusively. Equation (6) will be used in conjunction with Eq. (2) to evaluate the influence of three independent shape parameters,  $r_0$ ,  $r_1$  and V, on  $N_f$ .

#### Optimizing land (finger) and BLM dimensions

#### Theoretical considerations

It will be seen that the optimum interface dimensions  $r_0$  and  $r_1$  are virtually independent of solder volume, but that

the optimum volume is strongly a function of  $r_0$  and  $r_1$ . Thus the first step should be to optimize the two interface areas. Generally, one or the other will be fixed by design criteria; for the sake of illustration it will be assumed that the diameter of the ball-limiting metallization has been fixed. It can be shown that the ratio  $r_0/r_1$  is actually the optimizing parameter, so that the inverse procedure, choosing optimum  $r_1$  for fixed  $r_0$ , is exactly analogous.

From Eq. (2) it may be seen that although  $N_t$  is continuous with  $r_0$ , its first derivative is discontinuous (at  $r_0 = \sqrt{Kr_1}$ ) such that  $N_t$  cannot be maximized by calculus and must be evaluated numerically (graphically) for selected values of  $\tau_{ue}$ , V,  $r_1$ ,  $\beta$ , and K.

Figure 9 shows curves of  $N_f$  versus  $r_0$  for fixed values of K (1.563) and  $r_1$  (2 mils), and for three different values of V.  $N_f$  is normalized by dividing by those terms which are independent of pad geometry. Two points are significant: first the fatigue life for every chosen value of V (which encompasses the range of practical experimental values) is maximized at  $r_0 = \sqrt{K} r_1$ , the finger size for which the strengths of the two interfaces are equalized. Curves for other values of  $\beta$ , K, and  $r_1$  confirm this fact, namely that the optimum finger size is that for which the interface strengths are equalized, i.e.,

$$r_0^* = \sqrt{K} r_1, \tag{7}$$

and is independent of V and  $\beta$ .

The second point is the relative insensitivity of  $N_f$  to volume changes (the small differences among the three curves of Fig. 9) and the comparatively greater effect of finger size. Note, for instance, that at  $r_0 = 3$  and V = 60, increasing the volume by 50% (to V = 90) improves fatigue life by only 33%; while decreasing finger size 17% (to  $r_0 = 2.5$ ) improves fatigue life 100%. This point will be amplified in the following section.

Note that  $r_0$  influences  $N_f$  in two ways: it affects the ultimate strength (if  $r_0 < r_0^*$ ); and it affects the stiffness, since the ratio  $h^{1+\beta}/V$  is a function of  $r_0$ , as seen in Eq. (6). The interaction of these two factors is shown schematically in Fig. 10. The ultimate strength is constant above  $r_0^*$  but decreases rapidly below  $r_0^*$ . The compliance meanwhile is a constantly decreasing function of  $r_0$ . The product representing the combined effect resembles the curves in Fig. 9. (The hypothetical effect of sharp contact angles on the ultimate strength is also indicated.)

If design constraints fix the land size, but allow variation in the BLM diameter, it is easily seen that

$$r_1^* = r_0 / \sqrt{K},$$
 (8)

where the asterisk again denotes optimization.

#### Experimental evaluation of $r_0^*$ or K

It is apparent that the value of K and of  $r_0^*$  are very much functions of process parameters, e.g., electrode composi-

tion, firing temperature, and height; tinning; substrate preparation; intermetallic structure near the chip-joint interface, etc. Thus a method is necessary to experimentally determine the proper design value of  $r_0^*$  (or  $r_1^*$ ) for a particular fabrication sequence.

The most rigorous experimental technique to determine  $r_0^*$  would be to prepare samples identical except for varying finger size and subject them to successive machine (or as a substitute, thermal chamber) cycles and determine failure rates for each. If a sufficient variety of sizes were not available, fitting the data to the theoretical curve (Fig. 9) should prove sufficiently accurate. At any rate, however, sizes should be included on both sides of the estimated optimum. In lieu of fatigue cycling, the torque test is suggested as an appropriate and simple technique to achieve the same purpose with no more than a small error at most. The torque test may be legitimately used to determine  $r_0^*$ , with the assumption that the fracture mode is the same in torque as in thermal cycling, i.e., that the relative interface strengths are the same for both conditions. All experience to date has indicated that this is the case.

Curves similar to Figs. 9 and 10 can be derived for theoretical torque test data. Figure 11 shows theoretical values of  $T_m$  and  $\phi_m$ , with  $\sqrt{K} = 1.25$ ,  $\beta = 0.35$ ,  $r_1 = 2$  mils, and V = 65. The similarity to corresponding curves in Fig. 10 is obvious. The peaks on these curves are smoothed to indicate symbolically the fact that the torque test measures the average of many pads and the shift from all paste fractures to all chip fractures does not occur at a single finger size.

To use the torque test in determining optimum finger size, samples should be prepared having a range of finger sizes, but nominally identical in every other way. The best method would be simply to use different masks for screening. Care must be taken that the land height is the same in every case, since differences in land height are known to affect the paste-substrate adhesion  $\tau_{us}$ . Then, following tinning, identical chips should be joined to all samples in the same joining cycle, and the joints torque tested to determine  $r_0^*$ . Tests of this type are in progress, but data are not yet available.

If complete data of the type described above cannot be obtained, a rough approximation for  $r_0^*$  can be obtained if only two finger sizes are available, so long as one lies well below  $r_0^*$  and produces paste failures almost exclusively on torque test, and the other is well above  $r_0^*$  resulting in almost 100% chip failures. If the first test is denoted by subscript 1 and the second by subscript 2, then

$$\tau_{us}\pi r_{0_1}^2 = T_{m_1},$$

and

$$\tau_{uc}\pi r_1^2 = T_{max}$$

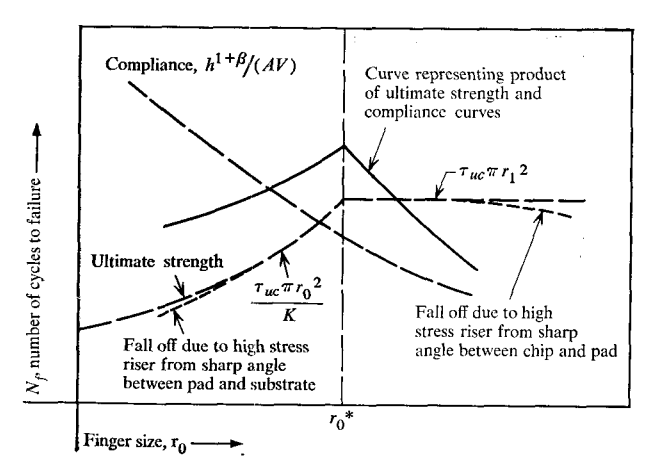
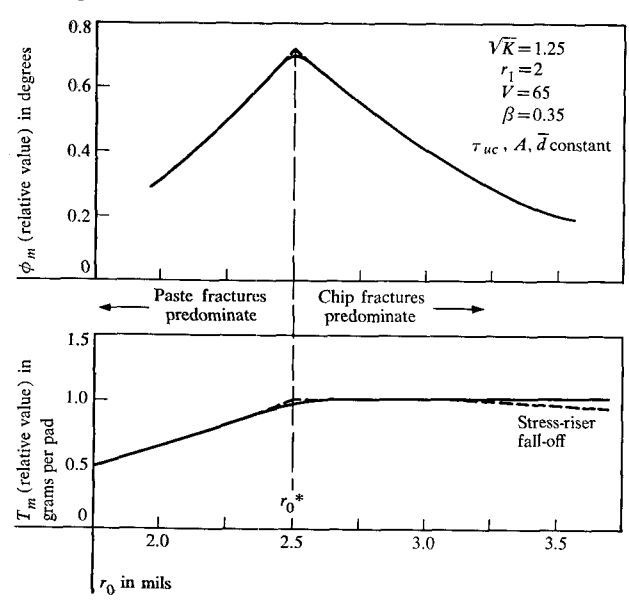


Figure 10 Ultimate strength and stiffness effects in joint fatigue.

Figure 11 Theoretical values of torque test measurements vs. finger size.



where  $\tau_{u_{\bullet}}$  and  $\tau_{u_{\epsilon}}$  are the ultimate shear strengths in lb/in<sup>2</sup> of the paste and chip interfaces respectively, and  $r_1$ , the BLM radius, is the same in both cases. Substituting  $\tau_{u_{\bullet}} = \tau_{u_{\epsilon}}/K$ , we have

$$(r_0^*)^2 = Kr_1^2 = r_{0_1}^2(T_{m_2}/T_{m_1}), (9)$$

which gives an approximate value for K.

Data are shown in Table 2 on two designs having the desired failure mode characteristics. Since the two designs used different chip sizes, the requirement of identical production procedures is not fulfilled, although corresponding steps in each sequence were nominally the same. The data therefore can serve to obtain an estimate of K, and in addition to illustrate the method.

Table 2 Torque test data for approximate determination

Design	r <sub>1</sub> , mils	Finger size, mils	r <sub>0</sub> , mils	$T_m$ , grams shear load per pad (average)	
	2.0	4 × 4	2.0	20.4	1.0%
2	2.0	$6 \times 6$	3.0	32.5	100.0%

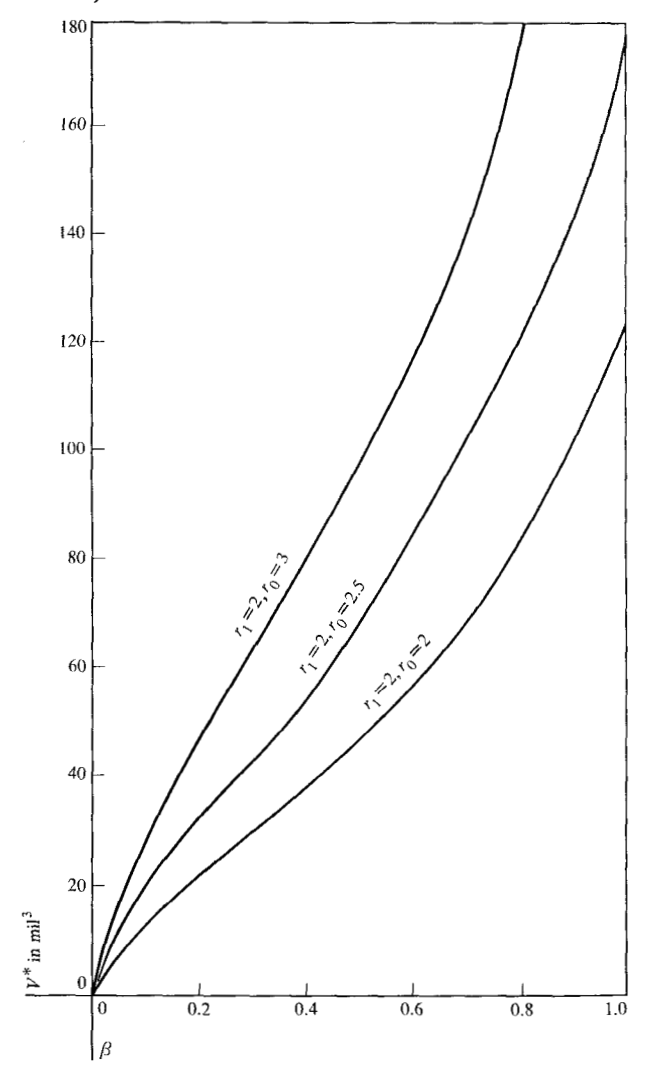
Substituting the values of Table 2 into Eq. (9) yields

K = 1.59.

 $r_0^* = 2.525 (5.05 \times 5.05 \text{ fingers}).$ 

Thus, for the fabrication technique investigated, the optimum value of the ratio  $r_0/r_1$  is approximately 5:4.

Figure 12 Design curves of  $V^*$  vs.  $\beta$  (optimum joint solder volume).



#### Optimizing volume and height

Expressions for h\* and V\*

Returning now to Eq. (2), with values of  $r_0$  and  $r_1$  decided upon (hopefully optimized, but not necessary for volume optimization), we note that the only geometric term remaining is the stiffness parameter  $h^{1+\beta}/VA$ . Since A is a material constant, it remains to maximize the ratio  $h^{1+\beta}/V$ , with the aid of the shape relationship, Eq. (6).

In Equation (6), when h is very small compared to 3  $(r_0^2 + r_1^2)$ , V increases directly as h and the ratio  $h^{1+\beta}/V$ increases with increased height. When h is large compared to  $3(r_0^2 + r_1^2)$  however, V approaches the third power of h and  $h^{1+\beta}/V$  decreases. Optimum values of V and h are thus directly implied, and are defined as  $V^*$  and  $h^*$ . When  $h < h^*$ , increasing volume increases height and produces a more flexible joint. When  $h > h^*$ , increasing volume continues to increase h, but a section through the main body of the joint is so much larger than the interface sections that most of the thermal displacement is borne by the solder near the top and bottom interfaces, and the gross pad stiffness increases.

Substitution of Eq. (6) into  $h^{1+\beta}/V$  and differentiation with respect to h yields the following optimum values\*:

$$h^* = \{ [3\beta/(2-\beta)](r_0^2 + r_1^2) \}^{\frac{1}{2}}, \tag{10}$$

$$V^* = [\pi/(2-\beta)][3\beta/(2-\beta)]^{\frac{1}{2}}(r_0^2 + r_1^2)^{\frac{3}{2}}.$$
 (11)

Curves of  $V^*$  against  $\beta$  for three different finger sizes  $(4 \times 4, 5 \times 5, 6 \times 6)$  with a 4 mil BLM diameter are shown in Fig. 12. It is apparent that the value of  $\beta$  has a very strong effect on  $h^*$  and  $V^*$ .

If the optimum values are substituted into Eq. (1),

$$N_{f}^{*} = K_{T} \cdot \left\{ \frac{\tau_{w} r_{f}^{2}}{A} \left[ (2 - \beta) \left( \frac{3\beta}{2 - \beta} \right)^{\beta/2} (r_{0}^{2} + r_{1}^{2})^{(\beta - 2)/2} \right] \right\}^{m/\beta} \left( \frac{1}{\delta} \right)^{m}.$$
(12)

$$(h^*)^3\!\!\left(\!\frac{2-\beta}{3}\!\right)-\,(h^*)^2h_p\,-\,h^*_1\!\beta(r_0^2\,+\,r_1^2)\,-\,h_p[r_1^2\,-\,(2\beta\,+\,1)r_0^2]\,=\,0\,,$$

where  $h_p$  is the average finger height. The idealized shape relationship (Eq. (6)) implies that  $V^*$  is independent of land height. This is true only for high values of  $\beta$  or for very low land heights. When  $\beta$  is less than 0.5 or when the finger height is more than 10 microns, the assumption is not valid, and the more complex expression must be used to obtain  $ht^*$ ; then  $Vt^*$  is found from Eq. (5), and the land volume subtracted from  $V_t$ \* to obtain V\*

A typical numerical example  $(r_0 = 3, r_1 = 2)$  shows that if  $\beta = 0.6$ , the error in  $V^*$  incurred by using Eq. (11) is 9.4% with a 30 micron land height and 3.1% with a 15 micron land height. If  $\beta = 0.4$ , the error is 175% for 30 microns, 19% for 15 microns, and 14% for 10 microns.

We may conclude from this discussion that the approximate  $V^*$ , Eq. (11) is entirely adequate for optimizing the joint with respect to machine thermal cycles, since for typical machine cycle strains, the design value of  $\beta$  is about 0.6, as will be shown in the following section. However, it is apparent that torque test data cannot be predicted by the approximate equation, since at  $\phi_m$ ,  $\beta$  is certainly at its minimum value of about 0.35. Moreover, it follows that the torque test cannot be used for volume optimization.

It will be recalled that the optimum interface dimensions  $(r_0^* \text{ or } r_1^*)$  are independent of  $\beta$ , which justifies use of the torque test for determining  $r_0^*$  or

<sup>\*</sup> If Eq. (5) is used instead of (6), thus including the land height and land volume in the calculations, differentiation of  $h^{1+\beta}/V$  yields the following complicated expression for the optimum chip-to-substrate height,  $h_t$ \*:

It may be shown that the indicated expression varies between 1.50 and 1.67 for all  $\beta$  values of interest. Thus to a rough approximation\*

$$N_f^* = K_T \left[ \frac{8}{5} \frac{\tau_u r_f^2}{A} (r_0^2 + r_1^2)^{(\beta - 2)/2} \right]^{m/\beta} \left( \frac{1}{\delta} \right)^m. \tag{13}$$

Flexibility in choosing h\* or V\*

If the optimum volume is not achieved, the interface stresses and strains due to a thermal perturbation will be larger than the theoretically calculated minimum, and the cyclic fatigue life will be reduced. The decrease in reliability may be found by substituting Eq. (12) into Eq. (1). After manipulation,

$$\frac{N_f}{N_f^*} = \left[\frac{R_h^{\beta}}{1 + \beta/2(R_h^2 - 1)}\right]^{m/\beta},\tag{14}$$

where  $R_h = h/h^*$ . Further manipulation yields

$$R_{v} = \left(\frac{N_{f}^{*}}{N}\right)^{\beta/m} R_{h}^{1+\beta}, \qquad (15)$$

where  $R_{\bullet} = V/V^*$ .  $R_{\bullet}$  is plotted against  $N_f/N_f^*$  in Fig. 13, for different values of  $\beta$ , and with m=2. From these graphs it is seen that relatively large deviations from the optimum volume cause only small changes in fatigue life. For instance, if  $\beta = \frac{2}{3}$ , the volume can vary from  $0.64V^*$  to  $1.62V^*$  (a factor of 2.5) with only a 10% drop in  $N_f$  from the optimum. The large "bandwidth" allows considerable leeway in joint design, and insures that if the nominal design volume is set at  $V^*$ , normal fabrication variations can be tolerated. Also, this flexibility can be used to advantage if  $\beta$  is unknown or variable, as is described in the following paragraphs.

#### Choosing an appropriate value of $\beta$

As is obvious from Fig. 12, the value of the strain-hardening exponent has a strong influence on the optimum pad dimensions. At present an appropriate value is not known. As may be seen from Fig. 2,  $\beta$  is not really a constant, but varies with shear strain. Within the elastic range  $\beta=1$ ; then it decreases in the transition region, reaching a minimum value, at which it remains constant over a large strain range. Torque test curves and data analyzed in the manner of Fig. 8 indicate a minimum  $\beta$  of about 0.35. Axial tensile tests on bulk 5/95 Sn/Pb solder<sup>4</sup> have shown a  $\beta$  of 0.14 for the ( $\alpha + \beta$ ) structure and 0.30 for the  $\alpha$  structure, for strains above 5%. The difficulty in assigning a particular  $\beta$  lies in the fact that for typical machine cycles, and chip sizes in the range 40  $\times$  60 to 110  $\times$  110 mils, the

$$\gamma^* = \left(\frac{r^*}{A}\right)^{1/\beta} \approx \delta \left(\frac{5/8}{r_t^2(r_0^2 + r_1^2)^{(\beta-2)/2}}\right)^{1/\beta}$$

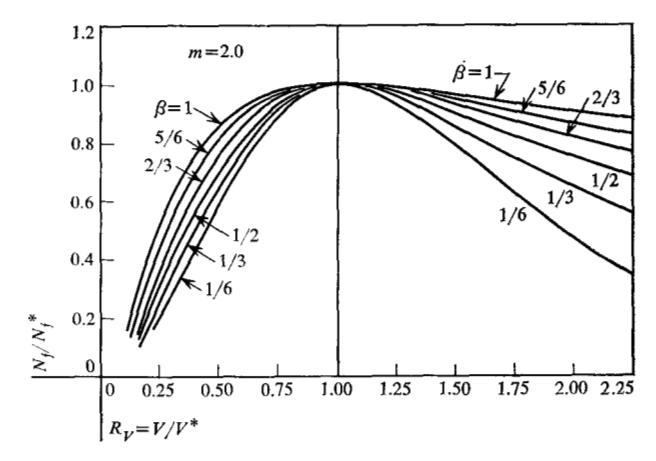


Figure 13 Curves of  $N_t/N_t^*$  versus  $R_v$ .

average shear strain amplitude on the corner pads is roughly in the range 0.3 to 0.6%, placing it most likely in the transition region. Moreover the elastic limit is a function of temperature and of strain rate. Finally, the cyclic  $\beta$  may not be the same as the single-cycle  $\beta$ . Evidently a good deal more experimentation is necessary before an accurate and appropriate value of  $\beta$  can be determined.

The wide "bandwidth" of the  $N_f$ -volume curve (Fig. 13) allows us to selectively choose an average working value of  $\beta$  that will minimize the deviation from  $N_f^*$  for the entire possible range of  $\beta$  encountered.

Assume that in all pads, throughout all cycles in a machine lifetime, the maximum  $\beta$  that will be encountered is 1.0 (elastic) and the minimum is  $\beta'$  (fully plastic). Then there is some value,  $\beta_d$  with  $\beta' < \beta_d < 1.0$ , which will minimize the deviation from  $N_f^*$  at the extremes. A value for  $\beta_d$  will now be derived.

Assume that  $\beta_d$  is known; then the height chosen, h, will be that given by Eq. (10), with  $\beta = \beta_d$ . At the extreme temperatures in a machine or thermal cycle, there will be some pad almost in the elastic state, i.e., with  $\beta \approx 1$ . This pad, if it were to be optimized, should have a height  $h^*$  equal to

$$h^* = [3(r_0^2 + r_1^2)]^{\frac{1}{2}}.$$

However its actual value is h as determined before; so that for this pad

$$h/h^* = h/h^* = [\beta_d/(2 - \beta_d)]^{\frac{1}{2}},$$
 (a)

and by Eq. (14)

$$\frac{N_f}{N_f^*} = \left\{ \frac{\left[\beta_d/(2 - \beta_d)\right]^{\frac{1}{2}}}{1 + \frac{1}{2}\left[\beta_d/(2 - \beta_d) - 1\right]} \right\}^m$$
 (b)

On the other extreme, some pad will be strained to the extent that  $\beta \approx \beta'$ . Thus for this pad

$$h/h^* = \bar{h}/h^* = \left\{ \frac{[\beta_d/(2-\beta_d)]}{[\beta'/(2-\beta')]} \right\}^{\frac{1}{2}},$$
 (c)

<sup>\*</sup> Note that Eq. (13) can be divided into local stress and strain components:  $\tau^* \approx \frac{5}{8} \frac{A \delta^2}{r_1^2 (r_0^2 + r_1^2)^{(\beta - 2)/2}};$ 

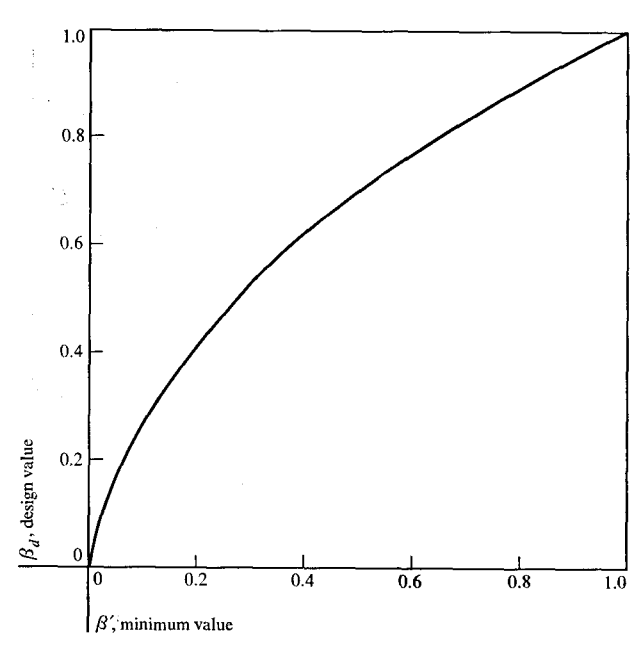


Figure 14 Design values for  $\beta$  to minimize drop-off from optimum fatigue life in extreme cases. Maximum  $\beta$  anticipated in machine environment: 1.0; Minimum  $\beta$  anticipated in machine environment:  $\beta'$ .

and by Eq. (14)

$$\frac{N_f}{N_f^*} = \left[ \frac{[\beta_d(2-\beta')/\beta'(2-\beta_d)]^{\beta'/2}}{1 + (\beta'/2)\{[\beta_d(2-\beta')/\beta'(2-\beta_d)] - 1\}} \right]^{m/\beta'}.$$
(d)

To minimize the deviation from  $N_f^*$  within the encountered range of  $\beta$ , it is necessary that the fatigue life at the two endpoints be equalized, i.e., that  $N_f/N_f^*$  of Eqs. (b) and (d) be set equal. The ensuing algebra results in an equation for  $\beta_d$ 

$$\beta_d = 2\{1 - \frac{1}{2}[(2 - \beta')^{(2-\beta')/(1-\beta)}(\beta')^{\beta'/(1-\beta')}]^{\frac{1}{2}}\}. (16)$$

This relationship is plotted in Fig. 14. For example if the minimum expected  $\beta$  is 0.35, then the design value should be 0.58. With values  $r_0 = 3$ ,  $r_1 = 2$ , this leads to an optimum volume (Fig. 12) of 112 mil<sup>3</sup>, corresponding to a solder height of 4.0 mils.

#### • Experimental correlation of optimization

Controlled tests with varying geometric parameters to verify theoretical optimization have not been completed, although such tests are currently underway. Limited data are available, however, for three specific designs that tend to confirm the model. A particular design  $(r_0 = 3, r_1 = 2, V = 60)$  with a median failure  $N_f$  of 3400 thermal cycles<sup>7</sup>

from 0 to 150°C was chosen as datum. Comparative calculated and experimental  $N_f$  values for the other two designs, having nominally the same material properties, are shown in Table 3.

#### • Optimum capabilities

If complete optimization is attained (assume the case where  $r_1$  is fixed), Eq. (2) reduces to

$$N_{f}^{*} = K_{T} \left[ (2 - \beta)^{1/\beta} \left( \frac{3\beta}{2 - \beta} \right)^{\frac{1}{2}} (K + 1)^{(\beta - 2)/2\beta} \cdot \left( \frac{r_{1}}{d} \frac{\tau_{uc}}{A} \frac{1}{\alpha \Delta T} \right)^{\frac{m}{2}} ,$$
 (17)

or approximately

$$N_f^* \approx K_T \left\{ \left[ \frac{8}{5(K+1)} \right]^{1/\beta} (K+1)^{\frac{1}{2}} \left( \frac{r_1}{d} \frac{\tau_{uc}}{A} \frac{1}{\alpha \Delta T} \right) \right\}^m.$$
 (18)

From this equation several conclusions can be reached:

- (1) A highly ductile solder (low A and  $\beta$ ) is desirable.
- (2) Also desirable are high  $\tau_{uc}$  and low K (high  $\tau_{us}$ ). (The parameter  $(\beta-2)/2\beta$  is always negative.) Thus the combined criteria of joint compliance and interface strength apply to material properties as well as to dimensional optimization.
- (3) There is an optimum chip size beyond which the cost benefits of higher circuit density are offset by the cost of module repair. It may be seen from the final equations that the cyclic fatigue life of an optimized joint still depends on two factors: material properties  $(A, \beta, \tau_{uc}, K, \alpha)$ and the ratio  $r_1/d$ , where d, the distance from the neutral point to the furthest pad, is a measure of chip size, and  $r_1$ is the radius of the chip-pad (BLM) interface. Consider the example cited earlier in which  $r_1 = 2$  and the optimized land radius and volume are  $r_0^* = 2.5$  and  $V^* = 81$ . Assume now that the chip must be enlarged so that d is increased by 50 percent. The joint designer could now take any of several courses of action. One possibility would be not to change the joint dimensions, in which case he would expect about a 56 percent decrease in module machine life (using m = 2). On the other hand, the same reliability could be maintained if  $r_1$  were increased proportionately as d and the other dimensions changed to maintain optimization. Thus  $r_1$  would have to increase, to 3 mils,  $r_0^*$  - by Eq. (7) - would also have to increase, to 3.75 mils  $(7.5 \times 7.5 \text{ fingers})$ , and  $V^*$  – by Eq. (11) – would have to increase by a factor of (1.5)3, to 273 mil3. This would in turn require larger spacing between joints (and hence fewer pads) and would consume more of the available chip area, thus negating the benefit derived from the larger chip. The designer's most likely choice would be to allow a small

Table 3 Experimental verification of geometric optimization.

Design	Finger Size mils	r <sub>0</sub> , mils	$r_1,$ $mils$	V, mil³	$N_f$ , calculated ( $\beta = 0.58$ , $m = 1.9$ )	$N_f$ , experimental <sup>7</sup>	% Error
1	6 × 6	3.0	2.0	60		3400	
2	$6 \times 6$	3.0	2.0	90	4240	4000	+ 6.0%
3	$7.5 \times 8$	3.76	2.0	60	824	1000	-17.6%

increase in the pad dimensions, so as to maintain the benefit of higher density, while accepting a definite but tolerable decrease in reliability. Beyond some chip size, however, the necessary decrease in reliability would offset the gain accrued from the increased number of circuits on the chip, and this condition defines the optimum chip size. This has been a very simplistic explanation; such factors as production costs, yield, and circuit speed will of course come into play and must be considered in any cost analysis.

#### Conclusions

Theoretical and experimental techniques have been introduced to analyze and evaluate the reliability of controlled collapse chip joints when subjected to cyclic thermally-induced strains. For given material properties, an optimum pad geometry exists; it may be determined by the following steps:

(1) Experimentally determine the value of K or  $\tau_{uc}/\tau_{us}$ 

via thermal cycling or a torque test, varying either BLM diameter or finger size, while keeping the other fixed. Once K has been determined, choose the largest BLM and finger size which chip or substrate constraints will allow, while maintaining the ratio  $r_0/r_1 = \sqrt{K}$ .

- (2) Determine a working value for the strain hardening exponent  $\beta$ , either by direct measurement at the proper strain ranges; or by the approximate technique described above.
- (3) Calculate the optimum solder volume from Eq. (11) or Fig. 12.

The torque test has been presented as a possible substitute for thermal cycling in estimating the cyclic fatigue life of the joint.

It bears repeating that the analysis presented is valid only when all joints on a pad are nominally identical. Other situations have been considered, but are beyond the scope of this paper.

#### Appendix A, fatigue life equation

For this analysis the pad is treated macroscopically as having gross properties. It is assumed that the Coffin-Manson relationship is valid for fixed thermal, machine or mechanical cycle.\* Then differences in fatigue life are due only to differences in the design tested. The number of cycles to failure,  $N_f$ , is given by<sup>†</sup>

$$N_f = \left(\frac{1}{\gamma}\right)^m \times C_T C_S \tag{A1}$$

where  $\gamma$  is the local shear strain at the critical point in the pad;  $C_T$  is a function of cycle temperatures, strain rates, and dwell times; and  $C_S$  is a function of material properties. If the same design is tested to destruction in a different

$$\frac{1}{2} = \left(\frac{1}{\gamma_u}\right)^m \times C_T'C_S,\tag{A2}$$

Where  $C'_T$  is a function only of the test cycle. Dividing (A1) by (A2), we have

$$N_f = 2 \frac{C_T}{C_T'} \left( \frac{\gamma_u}{\gamma} \right)^m \triangleq K_T \left( \frac{\gamma_u}{\gamma} \right)^m , \qquad (A3)$$

where  $K_T$  is a function\* only of the particular cycle and of the destructive test used to measure  $\gamma_u$ . This equation gives the number of cycles to failure in a particular thermal, machine, or mechanical cycle, when the local shear strain amplitude at the critical interface is  $\gamma$ , and where  $\gamma_u$  is

cycle, then failure occurs in  $\frac{1}{2}$  "cycle" when  $\gamma$  reaches  $\gamma_u$ , the ultimate strain. Thus

<sup>\*</sup> Norris and Landzberg² have confirmed the Coffin-Manson equation for the controlled collapse joint under thermal cycling conditions; they obtain a value of m of 1.9. Mechanical fatigue work by the author (unpublished) has also verified the exponential relationship between  $N_f$  and  $\gamma$ .

<sup>†</sup> We assume the plastic component of the strain to be much greater than the elastic component.

<sup>\*</sup>  $K_T$  includes the influences of strain rate, dwell times, and maximum temperature discussed in Ref. 2.

the ultimate strain (to fracture) of the same joint measured in a particular destructive test.

Fracture will begin at that cross-section at which the ratio  $\gamma_u/\gamma$  is a minimum, so the subscript f will be added to the ratio to denote the critical value. From a practical standpoint, fracture occurs generally at the land-ceramic interface or in the solder directly adjacent to the chip-pad interface. Then

$$N_f = K_T \left(\frac{\gamma_u}{\gamma}\right)_f^m \tag{A4}$$

The equation relating shear stress and shear strain is

$$\tau = A\gamma^{\beta},\tag{A5}$$

where A and  $\beta$  are constants. Equation (A4) thus becomes

$$N_f = K_T \left(\frac{\tau_u}{\tau}\right)_f^{m/\beta} \tag{A6}$$

Assume that the average shear stress and strain in the pad are related by Eq. (A5); that the average shear stress is simply the shear force F divided by the average solder cross-sectional area, V/h; and that the average shear strain\* is  $\delta/h$ . Thus

$$Fh/V = A(\delta/h)^{\beta}$$

or

$$F = [AV/(h^{1+\beta})]\delta^{\beta}. \tag{A7}$$

The average shear stress at an interface of circular crosssectional area  $\pi r^2$  is then

$$\tau = A\delta^{\beta}(V/\pi r^2 h^{1+\beta}). \tag{A8}$$

Substituting into (A6), we have

$$N_f = K_T \left[ \left( \frac{\tau_u \pi r_f^2}{A} \right) \left( \frac{h^{1+\beta}}{V} \right) \right]^{m/\beta} \left( \frac{1}{\delta} \right)^m \tag{A9}$$

where  $r_f$  is the radius at the critical point.

#### Appendix B, contact (re-entrant) angles

The question of contact angles has not been addressed in the main body of this paper since so many unknowns are still involved. That the normal stresses at the corners are significant in initiating fracture is beyond doubt.

$$N_f = K_T \left[ \left( \frac{\tau_u \pi \tau_f^2}{A} \right) \left( \frac{h^{1+\beta}}{V} \right) \right]^{m/\beta f} \left( \frac{1}{\delta} \right)^{m\beta/\beta f}$$

This would change the shape of the curves relating  $N_f$  to the various dimensions  $(r_1, r_6, V \text{ or } h)$  but would not affect the values of the optimized dimensions, since the term in brackets remains unchanged.

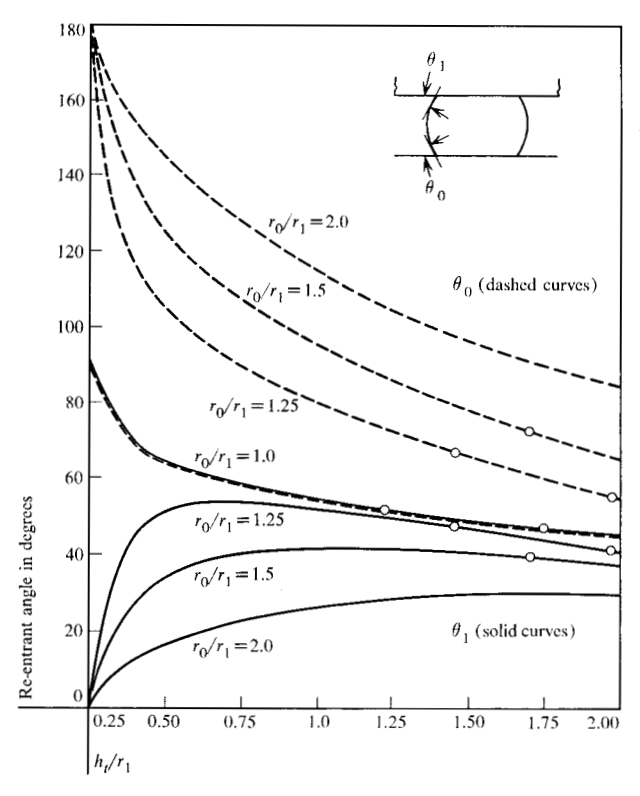


Figure 15 Curves of re-entrant angles  $\theta_1$  and  $\theta_0$  versus  $h_t/r_1$  ( $\bigcirc$  denotes point of optimum fatigue life).

What allows us to proceed as far as we have with shear strains and to claim their importance, effectively disregarding the effect of the normal strains, is the assumption that in plastic flow the normal strain increases with shear strain. Thus a pad with a higher shear strain at an interface than another pad exposed to the same temperature change also has higher normal strains at the corners.

If these two hypothetical pads also have very different re-entrant angles, however, these may also come into effect; and it is this difference with which we are concerned here. Two experiments<sup>5,6</sup> show that if the re-entrant angle is anywhere between about 30 and 90°, the "stress concentration" at the re-entrant corner is relatively independent of the angle, when the material is in the elastic range. This would indicate that the ratio of normal stress to shear stress is not likely to vary considerably with joint dimensions

A straightforward mathematical analysis has been derived to evaluate the contact angles  $\theta_0$  (at the substrate) and  $\theta_1$  (at the chip). It has been assumed that the pad has the shape of a spherical segment and that  $r_0 > r_1$ . The result:

$$\cos \theta_1 = \left[1 + 4\left(\frac{h_t}{r_1} - \frac{r_1}{h_t} + \frac{r_0^2}{r_1 h_t}\right)^{-2}\right]^{-\frac{1}{2}}, \quad (B1)$$

<sup>\*</sup> These approximations are least valid when the joint has large volume and small interfaces ("fat" pads), and when  $\beta$  is very small. They are sufficiently valid, in the region near optimized dimensions, that the simple derived relationships can be used with good accuracy. Exact solutions for pad stiffness and for local shear strains in the plastic range are available only in numerical form and thus not amenable to systematic optimization.

<sup>†</sup> A refinement can be made in the theory if in the immediate area of initial fracture, the solder is assumed more brittle than the bulk solder, i.e.,  $\beta_f > \beta$ . In this case (A9) would take the form

 $\cos \theta_0$ 

$$= \left\{1 - \left(\frac{r_0}{r_1}\right)^2 \left[1 + \frac{1}{4} \left(\frac{h_t}{r_1} - \frac{r_1}{h_t} + \frac{r_0^2}{r_1 h_t}\right)^2\right]^{-1}\right\}^{\frac{1}{2}} \cdot (B2)$$

The angles are related by

$$\sin \theta_1 = \frac{r_1}{r_0} \sin \theta_0. \tag{B3}$$

The angles are plotted against  $h_t/r_1$ , for different values of  $r_0/r_1$  in Fig. 15. The curves for  $r_0/r_1=1.0$ , 1.25, and 1.5 are all within the 30-90° range for  $(h_t/r_1) > 1.0$ —and the optimum value of  $r_0/r_1$  ( $\sqrt{K}$ ) certainly lies between 1.0 and 1.5. Moreover the curves, especially for the chip contact angle, are quite flat with  $h_t$ , and evaluation of  $h^*$  by Fig. 15 for the range of  $\beta$ ,  $r_1$ , and the land height of interest, shows  $h_t^*/r_1$  to lie on these flat portions. For instance, if  $\beta = \frac{2}{3}$ ,  $r_1 = 2$  mils, land height = 1 mil, the optimum values are indicated on the respective curves; all contact angles lie between 40° and 73°. Thus it is reasonable to assume that the contact angle criterion in no way contradicts the local shear strain criterion upon which dimensional optimization has been based.

#### **Acknowledgements**

The author wishes to thank L. J. Prescott, R. C. Yih, P. Lin, and F. J. Gude for the many discussions which led to this analysis; L. E. Liander, who designed the torque tester; and E. D. Renner, K. Wengier, and especially B. Krall who contributed greatly in perfecting the test apparatus and in collecting data.

#### References

- L. F. Miller, IBM J. Res. Develop. 13, 239 (1969, this issue.
- K. C. Norris and A. H. Landzberg, IBM, J. Res. Develop. 13, 266 (1969, this issue).
- S. S. Manson, Thermal Stress and Low Cycle Fatigue, McGraw-Hill Book Co., Inc., New York 1966, p. 132.
- 4. A. R. Edenfeld, private communication.
- A. J. Durelli, J. J. Parks and C. J. delRio, Experimental Mechanics, 7, 11 (1967).
- 6. C. Mylonas, Pros. SESA, XII, 2 (1954).
- 7. P. Lin, private communication.

Received December 11, 1968